Int. J. Electrochem. Sci., 15 **(2020)** 11868 – 11885, doi: 10.20964/2020.12.53

International Journal of ELECTROCHEMICAL SCIENCE
www.electrochemsci.org

Effect of Interaction between SDS and Tween 80 on Nucleation Behavior of Electrodeposited Copper Powder

Shuzhi Diao[1], *Yiyong Wang*[2,*], *Hui Jin* [3], *Jidong Li*[4], *Xianglin Liu* [5]

[1] School of Materials & Metallurgy, University of Science and Technology Liaoning, Anshan 114051, China
[2] School of Materials & Metallurgy, University of Science and Technology Liaoning, Anshan 114051, China
[3] School of Materials & Metallurgy, University of Science and Technology Liaoning, Anshan 114051, China
[4] School of Materials & Metallurgy, University of Science and Technology Liaoning, Anshan 114051, China
[5] School of Materials & Metallurgy, University of Science and Technology Liaoning, Anshan 114051, China
[*]E-mail: wangyiyongfly@163.com

Received: 8 January 2020 / *Accepted:* 14 August 2020 / *Published:* 31 October 2020

To study the electrochemical behavior of surfactants (sodium dodecyl sulfate (SDS) and Tween 80) during the deposition process, the electrocrystallization mechanism of copper powder was determined. Electrochemical test methods, such as linear sweep voltammetry (LSV), chronoamperometry (CA), and electrochemical impedance spectroscopy (EIS), were used. The kinetic parameters of the deposition process were calculated by the fitting experimental curves to verify the correctness of the theoretical analysis. The results show that the electrocrystallization process of copper conforms to the Scharifker-Hills 3D nucleation/growth mechanism. When the concentration of the surfactant was 0.2 g/L SDS+0.1 g/L Tween 80, the surfactant with a chain composite structure shifted the deposition potential negatively and increased the cathode polarization. The electrocrystallization of copper in the potential region from -0.20 V to -0.22 V was consistent with gradual nucleation, with a prolonged nucleation relaxation time and decreased nucleation rate. When the concentration of the surfactant was 0.8 g/L SDS+0.1 g/L Tween 80, the composite structure of the surfactant changed from long chains to spherical micelles. The spherical micelles positively shifted the deposition potential of copper and decreased the cathode polarization. Copper electrocrystallization in the potential region of -0.20 V to -0.22 V was consistent with instantaneous nucleation, the nucleation relaxation time was reduced, and the nucleation rate was accelerated. EIS showed that the surfactant Tween 80 formed a resistive film on the cathode surface. When 0.2 g/L SDS was added, the resistance R_1 of the resistive film increased; when SDS increased to 0.8 g/L, spherical micelles formed. Holes appeared in the resistive film, and its resistance decreased.

Keywords: Chronoamperometry; kinetic parameters; spherical micelles; resistance film

1. INTRODUCTION

Among various metal powders, copper powder is often used as an automotive lubricant additive because of its low price and excellent anti-friction properties. Not only does it prevent wear and tear on lubricated surfaces, it also increases the running speed and extends engine life [1-2]. Therefore, to improve the service life of engines, it is very important to analyze the performance of copper powder. The traditional preparation processes of copper powder mainly include the reduction method, electrodeposition method, physicochemical method and mechanical polishing method [3-5]. Among them, the preparation of copper powder by the electrodeposition method has the advantages of simple operation and a flexible process, which can not only efficiently recover Cu but also change the physical and chemical properties of copper powder by adjusting the electrochemical deposition parameters[6-7], such as the composition of the electrolyte, the role of the surfactant, the applied cathode current density, the solution temperature, and the pH value [8-10]. In addition, in the process of electrolytically preparing ultrafine powders, the electrocrystallization process on the substrate surface can be divided into two stages: nucleation and growth [11-12]. The competition between nucleation and growth determines the size and shape of the sediments, which affects the properties of copper powder. Therefore, the electrocrystallization process of ultrafine copper powder has been a research hotspot.

To obtain copper powder with an improved performance, various surfactants (MBT, SDS and Tween 80, for example) are usually added during the electrodeposition process [13-16]. Wenbo Lou et al. [17] studied the effects of potassium hexacyanoferrate and 2,2'-dipyridyl on copper electrodeposition, and the results showed that the two target-specific additives inhibited growth, which was conducive to obtaining fine spherical copper deposition products. Nekouie et al. [18] studied the effect of polyvinyl pyrrolidone (PVP) on copper electrodeposition behavior, and the results showed that PVP coordinates with copper, inhibits copper nucleation and refines the grains. Zheng J W et al. [19] demonstrated that the electrocrystallization process of copper follows a 3D transient nucleation/growth model controlled by diffusion. Although the above studies showed the effect of additives on copper powder, the electrocrystalline nucleation process of copper was also analyzed separately. However, the influence of additives on the nucleation process of copper powder is rarely analyzed, and specific kinetic parameters have not been calculated to analyze the electrocrystallization process.

In this paper, the initial deposition behavior of copper in a sodium lauryl sulfate-sulfuric acid system was studied, and the surface morphology and microstructure of the copper powder were characterized by scanning electron microscopy and X-ray diffraction. Cathode linear sweep voltammetry (LSV), chronoamperometry (CA) and other electrochemical test methods were used to record the electrocrystallization behavior of Cu. Finally, the nucleation process was simulated by an optimization algorithm, the kinetic parameters in the electrochemical reaction were calculated, and the nucleation mechanism of copper on the cathode surface in the presence of additives was determined and is explained. The nucleation mechanism of copper on the cathode surface was verified by AFM.

2. MATERIALS AND METHODS

During the preparation of copper powder, a stainless steel plate was used as the cathode with an effective area of 1 cm^2, and a platinum plate was used as the anode. Copper powder was prepared in a

300 mL electrolyzer. A high-frequency direct current powder (model PS-618) was used to apply a current density of 0.2 A/cm^2 during electrodeposition. An intelligent controlled temperature ultrasonic synthetic extractor (XH-2008DE model, Xianghu, Beijing, China) was used to maintain the temperature and had an ultrasonic power of 400 W with a frequency of 35 kHz during deposition. The chemical quantities and electrodeposition process parameters were as follows: the $CuSO_4$ was $5{\cdot}H_2O$ 0.05 g/L and the H_2SO_4 was 0.2 g/L; SDS and Tween 80 were also used. All electrolytes were prepared with analytical pure reagents and deionized water. The temperature of the electrolyte was 25 °C, and the pH value of the electrolyte was 2.1. Sonication occurred for 60 minutes.

An Autolab electrochemical workstation (AUT85731, Nova1.9, Metrohm, Switzerland) was used for the electrochemical measurements. In a three-electrode system, a copper plate was attached with electroplating glue and served as the working electrode (conducting area 1 cm^2), a platinum electrode was used as the counter electrode, and a saturated calomel electrode (SCE) was used as the reference electrode. All potential changes in the electrochemical test were relative to the reference electrode. The surface morphology and microstructure of the copper powder were observed using SEM (1 kV~15 kV, Zeiss-ΣIGMA HD, Carl Zeiss, Oberkochen, Germany). X-ray diffraction (X'Pert Powder, PANalytical, Almelo, The Netherlands) was used to study the preferred orientation of the deposits (Cu Kα filtered radiation, step size=0.02°, scan speed=10°/min, 2 theta ranged from 10° to 90°). The morphology of the copper powder was characterized by AFM (CSPM5500, Guangzhou, China), and the scanning area was 100 μm^2.

3. RESULTS AD DISCUSSION

3.1. Effect of SDS

To improve the size and agglomeration of the copper particles, SDS dispersants with different mass concentrations were introduced into the reduction system for direct current deposition. After the current efficiency was calculated by equation (1), the corresponding curves for the copper electrodeposition time and current efficiency were obtained, as shown in Figure 1:

$$CE = \frac{96485 \sum_{n=1}^{\infty} \frac{nm}{M}}{i \times t} \quad (1)$$

where CE is the current efficiency; 96485 C·mol^{-1} is the Faraday constant; n is the electron transfer number; m and M are the corresponding weight and molar mass of deposits, respectively; and i and t are the current and electrodeposition time, respectively [20].

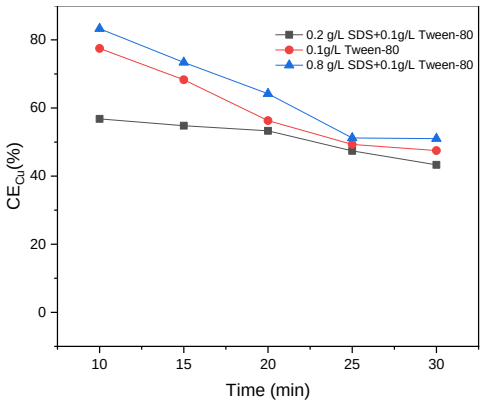

Figure 1. The relationship between the electrodeposition time and current efficiency for 30 minutes at T = 25 °C and pH = 2.1 in electrolytes with 0.1 g/L Tween 80, a 0.1 g/L Tween 80 + 0.2 g/L SDS, and 0.1 g/L Tween 80 + 0.8 g/L SDS.

Figure 1 shows that as the SDS concentration increases, the current efficiency decreases first and then increases. These experimental results are different from those in the literature [21]. Studies in the literature [21] used constant current experiments to show that when SDS was added to the acidic copper sulfate electrolyte, it suppressed the electrodeposition of copper and reduced the current efficiency. The reason is that SDS adsorption on the cathode surface reduced the effective area and mass transfer rate of the solution and reduced the current efficiency. However, we found that when the SDS concentration is increased to 0.8 g/L, the current efficiency significantly increases, mainly because when the SDS concentration increases to 0.8 g/L, the SDS and Tween 80 with long molecular chains form spherical micelles under the action of van der Waals forces [22]. The reaction principle is shown in Figure 2. The copper ions that are electrostatically adsorb on the spherical micelles experience a reduction reaction with the cathode. After the copper ions on the spherical micelles are reduced, the negatively charged spherical micelles are adsorbed on the surface of the copper particles [23-24]. Due to the repulsion effect, the spherical micelles that adsorb the copper particles are far away from the cathode surface, which reduces the adsorption of copper particles on the cathode surface and improves the current efficiency. Similar results were reported in the literature [25], which confirmed that different morphologies of surfactants can have different effects on the electrodeposition of copper powder.

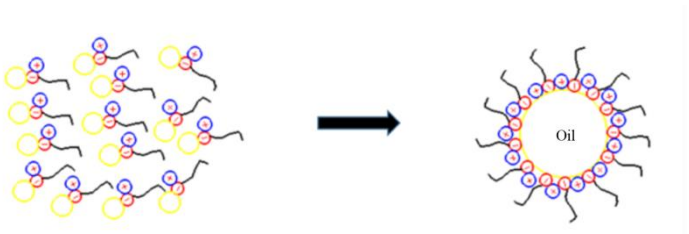

Figure 2. Principle of spherical micelle formation with 0.1 g/L Tween 80 and 0.8 g/L SDS at T=25°C and pH=2.1.

3.2. Linear Sweep Voltammetry

Figure 3 shows the linear sweep voltammetry of copper in the electrolytes with different surfactants. In the electrolyte with Tween 80, the initial deposition potential of copper on the cathode surface is approximately -0.16 V. In the electrolyte with 0.2 g/L SDS, the initial potential for the copper deposition is approximately -0.18 V. The addition of a small amount of SDS (no micelle formation) in the electrolyte negatively shifts the copper deposition starting potential and increases the cathode polarization. The negative shift of the reduction potential is mainly caused by the combination of long molecular chain SDS and Tween 80 that are adsorbed on the cathode surface, which reduces the effective area of the cathode and solution mass transfer rate and reduces the current efficiency [21]. However, when the concentration of SDS is 0.8 g/L (spherical micelle formation), the initial potential of the copper deposition shifts positively and the cathodic polarization decreases; this is mainly due to the principle of minimum energy formation. The surfactants in the solution form spherical micelles with positive static charges. After electrification, the spherical micelles move towards the cathode under the action of the electric field, and the hydrophilic groups adsorb Cu^{2+} to obtain electrons for the in situ reduction to elemental copper, at which time the static charge of the micelles is negative [26-27]. During the nucleation and crystallization of the powder, a spherical organic coating layer is formed on the surface of the metal crystal core according to the principle of minimum interfacial energy formation. Because the coating layer is negatively charged and the cathode is negatively charged, the adsorption capacity of the powder on the cathode decreases under the action of repulsion, resulting in an increase in the current density. The experimental results are consistent with those reported in [28-29].

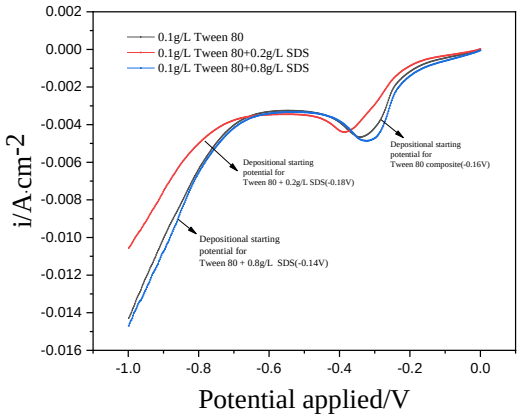

Figure 3. Linear sweep voltammetric curve obtained for electrolytes with 0.1 g/L Tween 80, 0.1 g/L Tween 80 + 0.2 g/L SDS, and 0.1 g/L Tween 80 + 0.8 g/L SDS at scanning potentials from 0 V to - 1 V at T= 25 ℃ and pH = 2.1.

3.3. Chronoamperometry Study

Chronoamperometry is an effective method to analyze the nucleation during metal electrocrystallization processes [30]. Figure 4 shows the chronoamperometry curves of copper at different step potentials in electrolytes with different surfactants. The step potential ranges from -0.2 V to -0.28 V.

The I ~ t curves in Figure 4 have 3D nucleation characteristics that are controlled by diffusion [30]. From the i ~ t curve, it can be seen that the current caused by the charge in the double charge layer first decreases and then increases, and then the current density controlled by the nucleation/growth of the crystal gradually increases and reaches the maximum value. Finally, the current density controlled by the cathode gradually decreases [30-31].

As seen from the curve in Figure 4, when the SDS concentration in solution increases gradually, the current peak decreases first and then increases, indicating that when SDS is 0.2 g/L, the chain-like composite structure formed by SDS and Tween 80 reduces the electric crystallization rate of the copper. When the SDS increases to 0.8 g/L, the composite structure changes from chain-like to spherical micelles, and spherical micelles increase the rate of copper electrocrystallization. It can also be observed in the figure that the transient current first rises rapidly and then decreases in a very short time after the potential step starts, and then the current gradually rises again, reaches a maximum value and then decreases. This feature is similar to that of Scharifker and Hill [30-31]. The characteristics of the three-dimensional multinuclear growth potentiostat I and t curve derived from diffusion control are consistent.

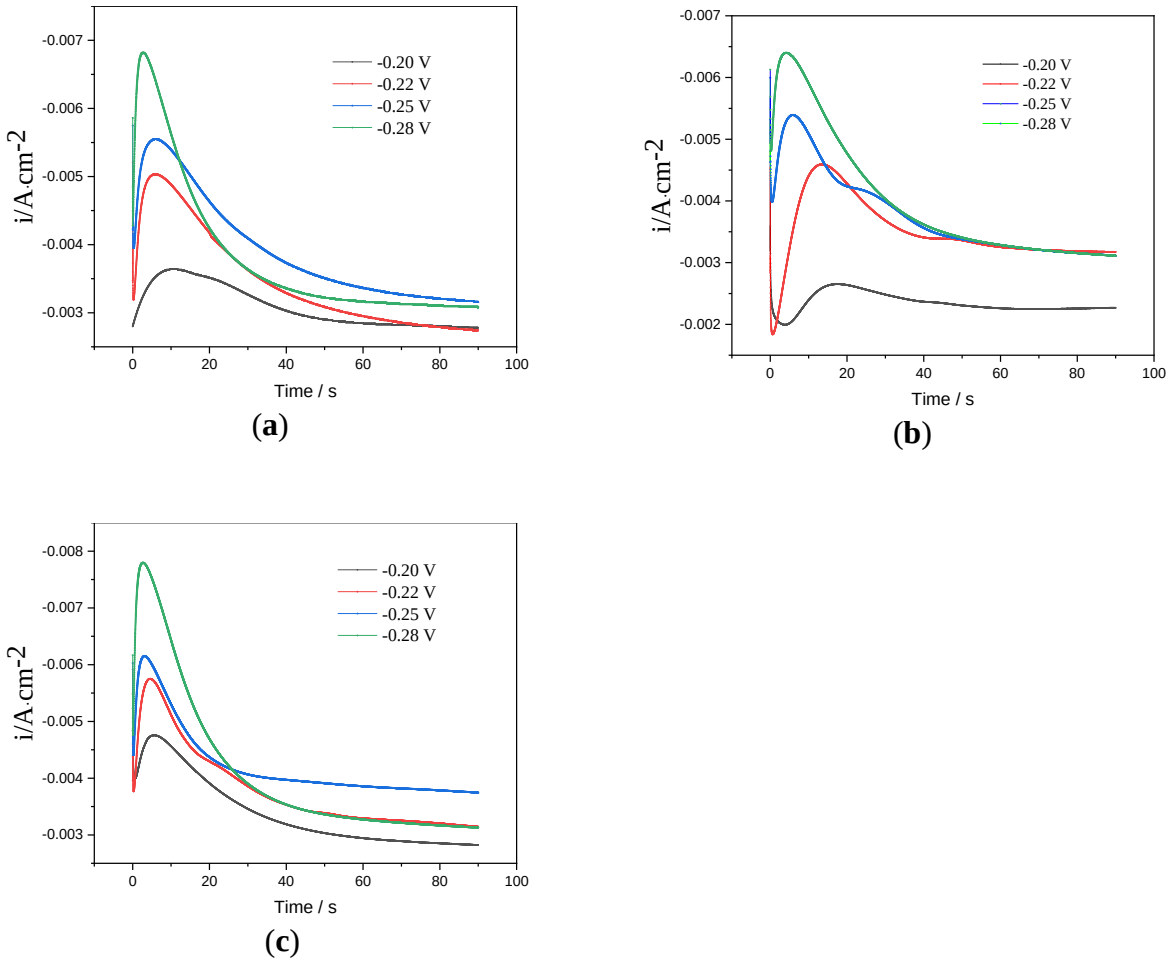

Figure 4. Current-time curves on the stainless steel electrode at a step potential from -0.2 V ~ -0.28 V, where T = 25 °C and pH = 2.1: (a) I ~ t curve of electrolyte with 0.1 g/L Tween 80, (b) I ~ t curve of electrolyte with 0.1 g/L Tween 80 + 0.2 g/L SDS mixture, and (c) I ~ t curve of electrolyte with 0.1 g/L Tween 80 + 0.8 g/L SDS mixture.

To describe the initial nucleation process of electrocrystallization, after processing the instantaneous nucleation in equation (2) and the gradual nucleation in equation (3), the results are compared with the Scharifker-Hills nucleation model [30] in Figure 4 to obtain the dimensionless (I/IM)2-t/tm curve, as shown in Figure 5:

$$(I/I_m)^2 = \frac{1.9542}{(t/t_m)}\left\{1-\exp\left[-1.2564(t/t_m)\right]\right\}^2 \quad (2)$$

$$(I/I_m)^2 = \frac{1.2254}{(t/t_m)}\left\{1-\exp\left[-2.3367(t/t_m)^2\right]\right\}^2 \quad (3)$$

where I and I_m represent the current density and the maximum value of the current density, respectively; and t and t_m represent the time and the time when the current density reaches the maximum value I_m, respectively.

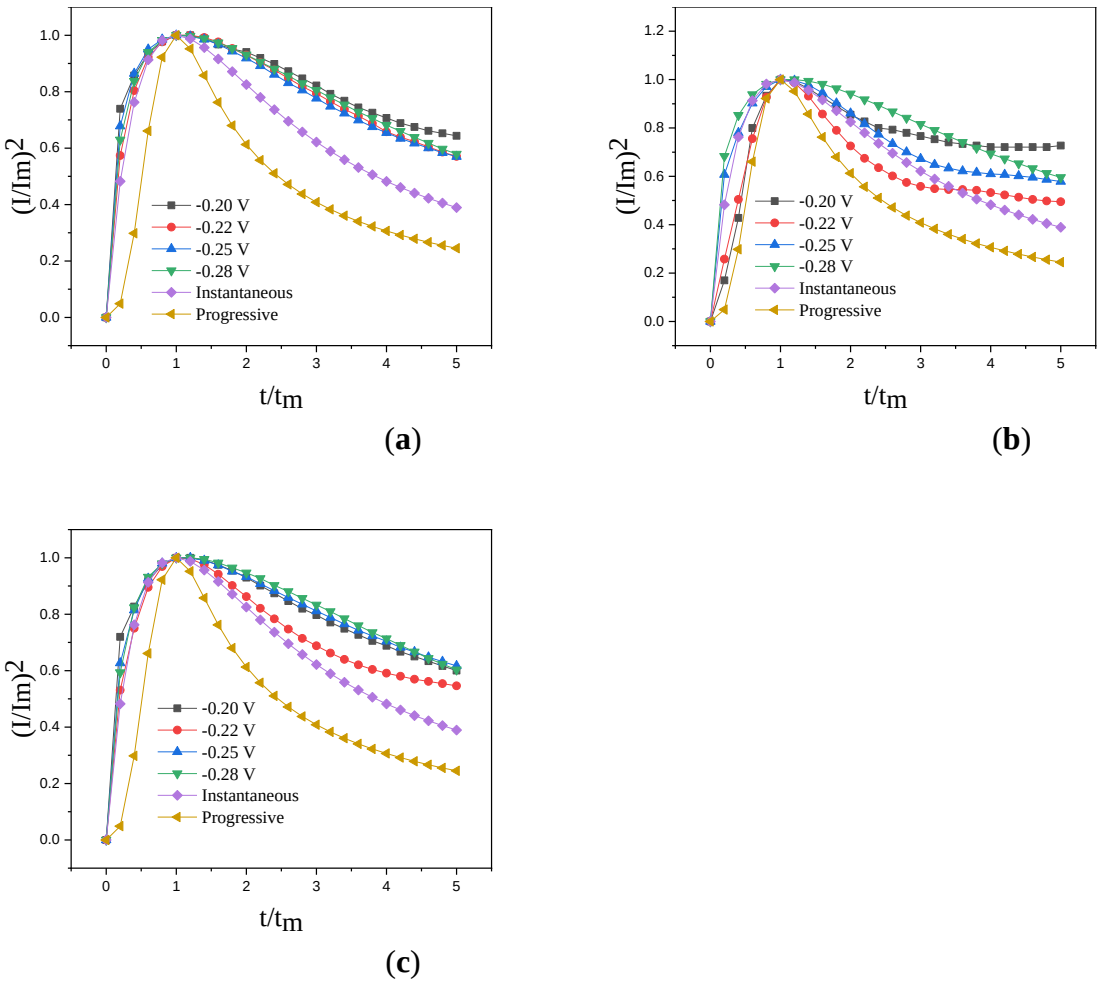

Figure 5. Curves corresponding the Scharifker-Hills model at T = 25℃ and pH = 2.1 and from -0.2 V ~ -0.28 V for electrolytes with (a) 0.1 g/L Tween 80, (b) 0.1 g/L Tween 80 + 0.2 g/L SDS mixture, and (c) 0.1 g/L Tween 80 + 0.8 g/L SDS mixture.

From Figure 5 (a), the dimensionless curve of copper is close to the instantaneous nucleation curve in the potential region from -0.2 V ~ -0.28 V. However, as shown in Figure 5 (b), when the SDS concentration is 0.2 g/L, the dimensionless curve of copper approaches a gradual nucleation curve in the potential region from -0.2 V to -0.22 V. From -0.25 V to -0.28 V, the dimensionless curve of copper is close to the instantaneous nucleation curve. This is different from the instantaneous nucleation curve of copper in reference [32]. This is because the energy of the active sites on the substrate surface is different. When chain-like SDS was added, the energy of the active sites was weakened, and copper nucleation was suppressed [32-33]. As shown in Figure 5 (c), when the SDS concentration is increased to 0.8 g/L, the dimensionless curve of copper in the potential region of -0.2 V to -0.28 V indicates instantaneous nucleation. The main reason is that the surfactant forms spherical micelles, which activate the active sites on the cathode surface and accelerate the nucleation and growth of the copper [34]. When $t/t_m > 1$, the test curve gradually deviates from the nucleation and dimensionless curve. The reason for the deviation is not yet clear. Radisic believes that the electrodeposition of copper generates hydrogen, which increases the fluid mass transfer on the cathode surface and causes a deviation in the curve [34]. However, this explanation is problematic because the larger the current density is, the more hydrogen is released, and the greater the deviation; this result is different from that in Figure 5. Therefore, the morphology of the nucleus is likely to explain the deviation. Since the nucleation model is derived for a hemispherical geometry, any behavior deviating from this morphology causes deviation from the model. This is consistent with the analysis of Darko Grujicic [32]. Moreover, the theoretical models of instantaneous nucleation and gradual nucleation are derived on the premise that the base surface is smooth, while the actual electrode surface has scratches and gaps, resulting in a deviation between the experimental curve and the theoretical curve. In summary, during electrodeposition, a reduction in the number of hydrogen ions and deposition of the matrix metals occurs simultaneously. In addition to the discharge of metal ions, hydrogen evolution also provides an additional current density. Therefore, during the analysis of the transient curves, the nucleation process of the matrix metals is considered as well as the effect of hydrogen evolution. Scharifker-Hills [30] and Palomar-Pardave [35] et al. also reached such a conclusion and further studied the metal deposition process affected by hydrogen evolution. Palomar-Pardave [35] proposed a formula for the total current density and nucleation parameters for the simultaneous electrocrystallization deposition of metals and hydrogen evolution reaction:

$$i(t)=\left\{P_1^{*}+P_4 t^{-\frac{1}{2}}\right\}\times\left\{1-\exp\left[-P_2\left(t-\frac{1-\exp(-P_3 t)}{P_3}\right)\right]\right\} \tag{4}$$

$$P_1^{*}=P_1\left(\frac{2CM}{\pi\rho}\right)^{\frac{1}{2}} \tag{5}$$

$$P_1=Z_{PR}FK_{PR} \tag{6}$$

$$P_2=N_0\pi KD \tag{7}$$

$$P_3=A \tag{8}$$

$$P_4=\left(\frac{2FD^{\frac{1}{2}}C}{\pi^{\frac{1}{2}}}\right) \tag{9}$$

$$K = \left(\frac{8\pi C}{\rho}\right)^{\frac{1}{2}} \quad (10)$$

where i is the current density, F is the Faraday constant, $Z_{PR}F$ is the molar charge during the reduction of hydrogen ions, K_{PR} is the hydrogen evolution reaction rate constant, M is the molecular mass, C is the molar concentration of ions in the electrolyte solution, D is the diffusion coefficient, A is the nucleation rate, and N_0 is the number of active sites.

Formula (4) is used to perform nonlinear fitting on the test transient curve to calculate P_1*, P_2, P_3, and P_4 [35]. Figure 6 shows the results of the nonlinear fitting between the experimental curves and theoretical curves of the different electrolytes at different step potentials. The fitting degree between the theoretical curve and the experimental curve is high, and the data calculated theoretically can be used to analyze the experimental curve. The results showed that the nucleation rate (P_3) of the copper in the electrolyte with an SDS concentration of 0.8 g/L was the fastest obtained herein, the nucleation rate of the copper in the electrolyte with Tween 80 was second.

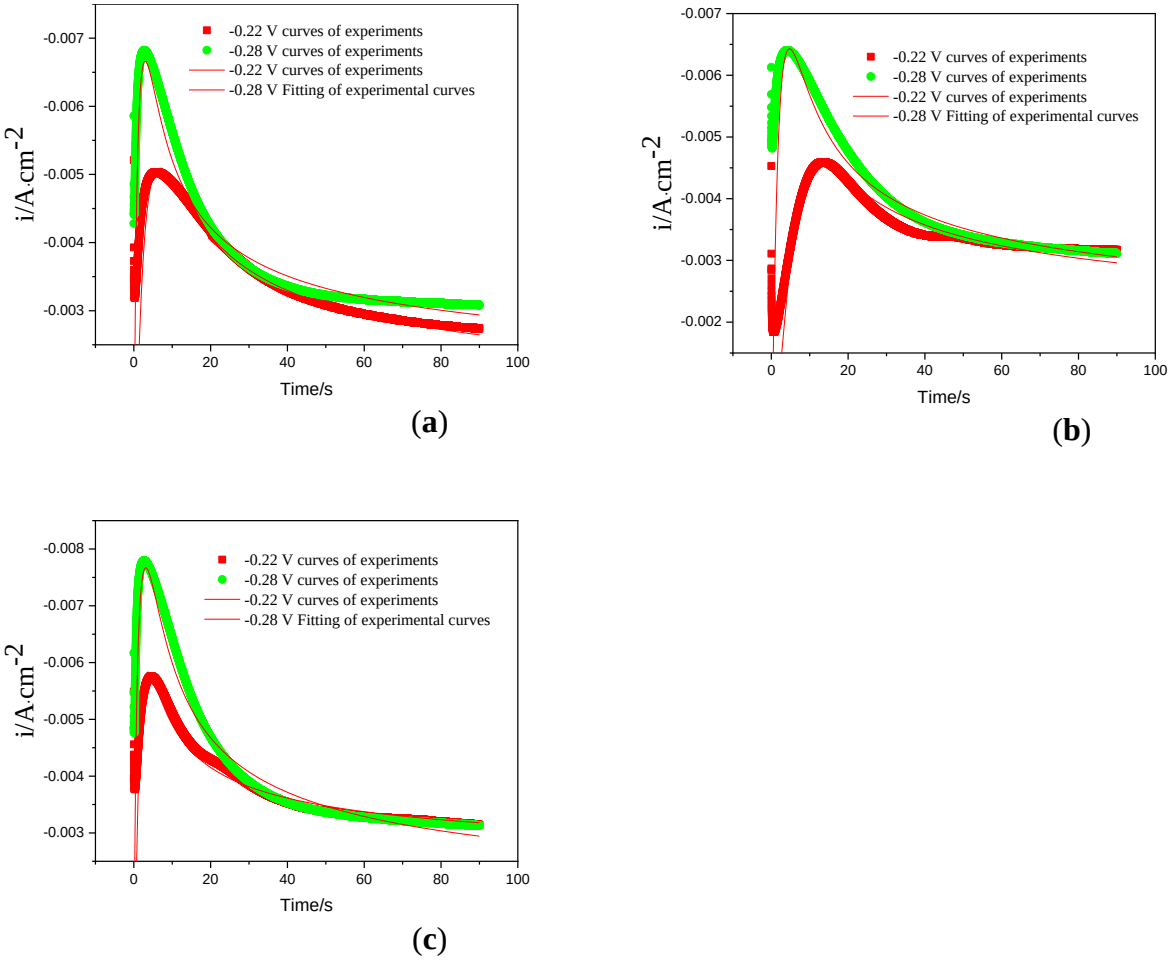

Figure 6. Transient curve and nonlinear fitting theoretical curve corresponding to T = 25 ℃ and pH = 2.1 under -0.2 V and -0.28 V for electrolytes with (a) 0.1 g/L Tween 80, (b) 0.1 g/L Tween 80 + 0.2 g/L SDS mixture, and (c) 0.1 g/L Tween 80 + 0.8 g/L SDS mixture.

It was proven that the chain-shaped surfactant could inhibit copper nucleation, and the spherical micelle-shaped surfactant could promote copper nucleation. The data calculated by the theoretical curve agree with the experimental results in Figure 3. The data are shown in Table 1.

Table 1. Results under the potentials of -0.22 V and -0.28 V at T = 25 ℃ and pH = 2.1 for electrolytes with (a) 0.1 g/L Tween 80, (b) 0.1 g/L Tween 80 + 0.2 g/L SDS mixture, and (c) 0.1 g/L Tween 80 + 0.8 g/L SDS mixture. The best nucleation kinetic parameters are deduced from formula (4).

Solution	Potential/V	P_1* （μA·cm^{-2}） ×10^{-3}	P_2 （s^{-1}）	P_3 （s^{-1}）	P_4 （μA·cm^{-2}）	A （s^{-1}）
0.1 g/L Tween 80	-0.22V	-1.34	0.30	1.41	-0.012	1.41
0.1 g/L Tween 80	-0.28V	-1.79	0.61	9.44	-0.011	9.44
0.1 g/L Tween 80+0.2 g/L SDS	-0.22V	-1.73	0.32	0.18	-0.011	0.18
0.1 g/L Tween 80+0.2 g/L SDS	-0.28V	-1.70	0.45	1.82	-0.013	1.82
0.1 g/L Tween 80+0.8 g/LSDS	-0.22V	-2.30	0.68	1.97	-0.0082	1.97
0.1 g/L Tween 80+0.8 g/L SDS	-0.28V	-1.40	0.52	10.78	-0.015	10.78

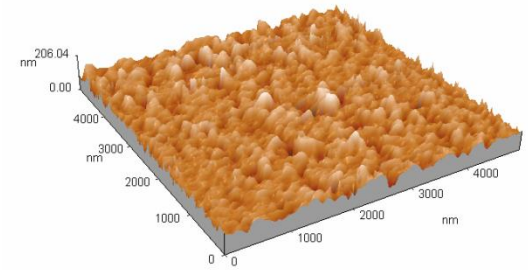

(**a**)

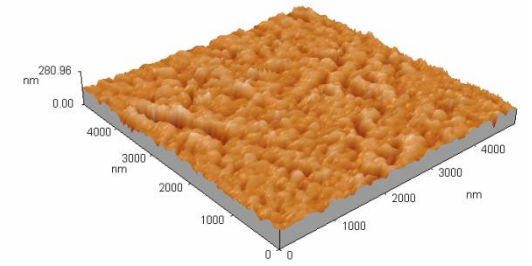

(**b**)

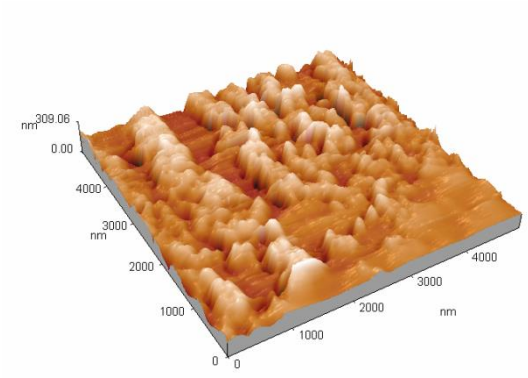

(**c**)

Figure 7. AFM images of copper electrodeposition for 30 s at a potential of -2.20 V (vs. SCE) at different SDS concentrations, T = 25 °C, and pH = 2.1 for electrolytes with (a) 0.1 g/L Tween 80 + 0.8 G/L SDS mixture, (b) 0.1 g/L Tween 80, and (c) 0.1 g/L Tween 80 + 0.2 g/L SDS mixture.

To study the deposition morphology of copper electrocrystallization on the substrate surface during the initial stage AFM was used to observe the copper powder electrodeposited at a potential of -2.2 V, as shown in Figure 7. As seen from Figure 7ac, the copper powder grown on the surface of the stainless steel is the most uniform in the electrolyte with 0.1 g/L Tween 80 + 0.8 g/L SDS, while in the electrolyte with 0.1 g/L Tween 80 + 0.2 g/L SDS, the copper powder that grows in is the roughest. As shown in Table 2, when the electrodeposition time is 30 s, copper nuclei grow most in the electrolyte with 0.1 g/L Tween 80 + 0.8 g/L SDS mainly because of a high nucleation rate (A) and additional active nucleation sites (N_0). In addition, the AFM images provide support for the calculated values of the number of nucleation active sites (N_0) and nucleation rate (A) in Table 1. However, the difference between the calculated nuclear diffusion densities is approximately an order of magnitude, which is several orders of magnitude higher than the data reported in [32]. The possible explanation for the difference is that the mathematical model cannot distinguish the nucleation phenomenon that occurs in the diffusion region because there are multiple nuclei in a diffusion region, for example [34].

Table 2. Particle sizes after deposition at the following conditions: the current density was 0.1 A/cm^2, T=25℃ and pH=2.1 for electrolytes with 0.1 g/L Tween 80, 0.1 g/L Tween 80 + 0.2 g/L SDS, and 0.1 g/L Tween 80 + 0.8 g/L SDS.

Solution	0.1g/LTween 80	0.1g/L Tween 80+0.2g/L SDS	0.1g/L Tween 80+0.8g/L SDS
The total number of particles	1600	1372	2771

3.4. Electrochemical Impedance Spectroscopy (EIS) Studies

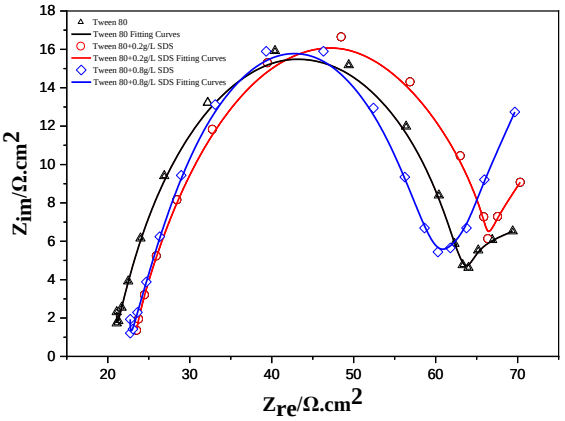

Figure 8. AC impedance spectrum in electrolytes at the same potential (-0.22 V), T = 25 ℃, and pH = 2.1 for electrolytes with 0.1 g/L Tween 80, 0.1 g/L Tween 80 + 0.2 g/L SDS, and 0.1 g/L Tween 80 + 0.8 g/L SDS.

Figure 8 is a Nyquist plot of the AC impedance spectra obtained in different electrolytes at a potential of -0.22 V. It is an approximate semicircular reactance arc at high frequencies. This indicates that the copper powder formation process of the studied system is controlled by charge transfer, and the

diameter of its semicircle corresponds to the electrochemical reaction charge transfer resistance. The larger the radius value is, the greater the resistance of the electrochemical process and the slower the reaction [35]. At low frequencies, the curve changes from a semicircle-circle to a Warburg impedance line with an inclination angle of nearly 45°, indicating the characteristics of diffusion control. Thus, the electrodeposition of Cu is controlled by diffusion at a potential of -0.22 V, which is consistent with the experimental results of the polarization curves. Capacitive arcs occur in the high frequency region, and Warburg impedances appear in the low frequency region. The reason for this phenomenon is that the electrode surface contains a film layer that absorbs the surfactant [36]. As the test time increases, a visible copper powder appears on the electrode surface. With the formation of the copper powder, the existing concentration gradient disappears, and due to the accelerated formation of the copper powder, a new concentration gradient layer is formed in the interface area [37]. This result reflects the Warburg impedance caused by the diffusion of copper ions from the inside of the surfactant film to the outside of the film.

Figure 9. The equivalent circuit that describes the negative resistor and negative capacitor components (a) at -0.22 V, T = 25 °C, and pH = 2.1, and the equivalent circuit (same as Figure 3 (a)) plus a Warburg component for (b) inductive behavior.

Table 3 The electrochemical parameters obtained by the equivalent circuit diagram in Figure 9 were fitted by Zview fitting software at a potential of - 0.22 V, T= 25 °C and pH = 2.1 for electrolytes with 0.1 g/L Tween 80, 0.1 g/L Tween 80 + 0.2 g/L SDS, and 0.1 g/L Tween 80 + 0.8 g/L SDS.

Solution	Potential	$R_s/\Omega.cm^2$	$CPE_1/F.cm^2$	$CPE_2/F.cm^2$	$R_t/\Omega.cm^2$	$R_1/\Omega.cm^2$	$W_1/\Omega.cm^2$
0.1 g/L Tween 80	-0.22V	16.66	5.59×10^{-4}	0.075	12.90	38.67	0.45
0.1 g/L Tween 80+0.2 g/L SDS	-0.22V	20.72	2.52×10^{-4}	0.088	18.22	44.61	0.193
0.1 g/L Tween 80+0.8 g/L SDS	-0.22V	31.45	6.96×10^{-4}	0.014	7.35	37.60	0.02758

Some researchers [38] used a circuit containing both a negative capacitor and a negative resistance (Figure 9 (a)) to describe the electrodeposition behavior. There is no obvious magnetic field

energy in front of the cathode to provide additional physical methods to represent the process leading to the inductive characteristics [38-39]. This article uses the equivalent circuit shown in Figure 9 (b).

The electrode process is mainly controlled by electrochemical steps. The equivalent circuit is shown in Figure 9, where R_s is the solution resistance, R_1 is the membrane resistance, CPE_2 is the interface capacitance of the surfactant film, R_t is the transfer resistance, CPE_1 is the electric double layer capacitance, and W_o is the diffusion process [39-40]. The electrochemical parameters obtained by fitting the impedance spectrum by the Zview fitting software using the equivalent circuit of Figure 9 are shown in Table 3.

As seen in Table 3, the electrode charge transfer resistance increases, and the interface capacitance decreases after 0.2 g/L SDS is added. This indicates that the additives have improved adsorption film-forming properties [36]. The electrode process is mainly controlled by electrochemical reactions. After adding 0.2 g/L SDS, R_1 gradually increases and CPE_2 gradually decreases. This shows that Tween 80 + 0.2 g/L SDS reacts on the electrode surface and adsorbs on the surface of the metal substrate to enhance the film formation ability. R_1 (membrane resistance) increases significantly with increasing SDS concentration; CPE_2 (interface capacitance of metal/solution film) tends to decrease, but the opposite is true when SDS concentration increases to 0.8 g/L. This is because as the concentration of SDS increases, spherical micelles are formed, resulting in voids on the electrode surface resistive film, and the film is not very dense. This is consistent with the results discussed in the literature [41]. The fitting calculation results are consistent with the theoretical analysis of the Nyquist spectra.

3.5. Microscopic morphology of the copper powder

X-ray diffraction analysis was performed on copper powders prepared in electrolytes with different mass concentrations of SDS + Tween 80, and the results are shown in Figure 10. When SDS is added, Cu diffraction peaks appear at 43.61°, 50.71°, 74.35°, 90.12° and 95.32°, corresponding to the (1 1 1), (2 0 0), (2 2 0), (3 1 1), and (2 2 2) crystal planes of Cu, respectively, indicating a high crystallinity. This shows that the sample with added SDS has an elevated purity and does not contain a substantial amount of impurities. This result is consistent with that of other studies [32]. Moreover, there is almost no difference between the A_1 and A_2 peaks, indicating that the addition of SDS does not affect the crystal structure of the Cu particles but only affects the morphology and composition of the Cu particles. However, it can be seen from line A_3 that when SDS is not added, a diffraction peak of Cu_2O appears at 36.65°, indicating that the addition of SDS can effectively prevent the oxidation of Cu particles in the solution. This may be because the combination of Cu and SDS Tween 80 hinders the contact of Cu particles with the remaining components in the solution, thereby achieving an antioxidant effect [42].

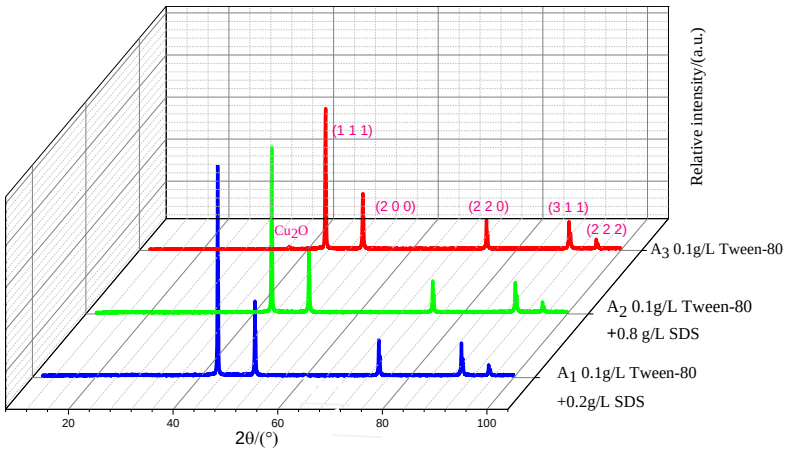

Figure 10 X-ray diffraction pattern of copper prepared in the electrolytes at a current density of 0.1 A/cm^2, T = 25 ℃, pH = 2.1 and with 0.1 g/L Tween 80, 0.1 g/L Tween 80 + 0.2 g/L SDS, and 0.1 g/L Tween 80 + 0.8 g/L.

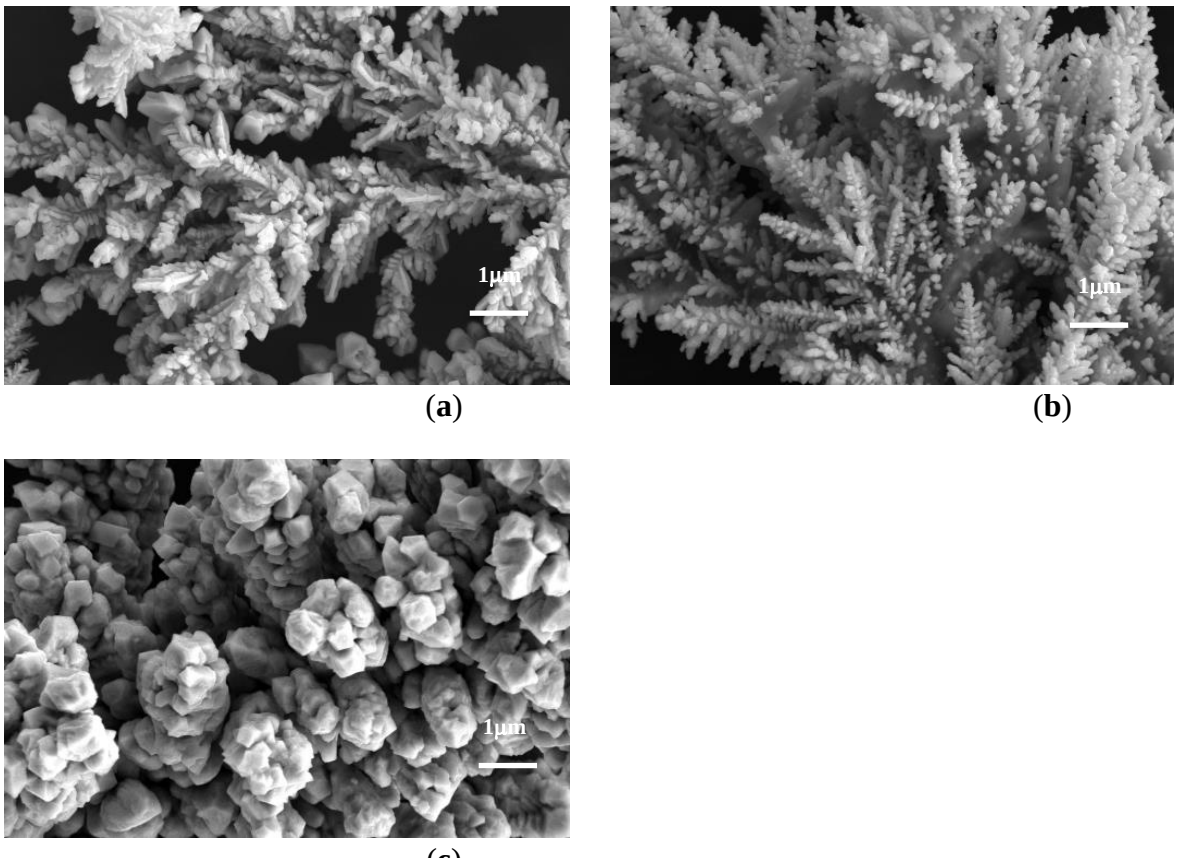

Figure 11. SEM images of copper powder prepared at a deposition current density of -0.1 A/cm^2, T = 25 ℃, pH = 2.1 and different SDS concentrations of (a) 0.1 g/L Tween 80, (b) 0.1 g/L Tween 80 + 0.2 g/L SDS, and (c) 0.1 g/L Tween 80 + 0.8 g/L SDS.

As shown in the SEM image in Figure 11 (a), the copper powder prepared in the electrolyte with Tween 80 shows that the copper powder has a dendritic shape. As shown in the SEM image in Figure 11 (b), the copper powder prepared with an SDS concentration of 0.2 g/L forms sharp features. This is

mainly because when a small amount of SDS does not form a concentration of spherical micelles, the chain-shaped composite organic compounds coated on the surface of the copper particles are unevenly distributed [43], which makes copper grow in preferred directions (see Figure 12 (a)). As shown in the SEM image in Figure 11 (c), where the SDS concentration is 0.8 g/L, the prepared copper powder is close to spherical in shape. This is mainly because when the concentration of SDS is 0.8 g/L, the surfactant molecules easily aggregate to form many spherical micelles with a net positive charge to reach their lowest energy level [26]. After being energized, these micelles move towards the cathode, trapping electrons and reducing Cu^{2+} ions in the pre-electrode layer. Copper molecules attracted by the active agent molecules collide with each other, causing the coalescence of the electrolyte to form a spherical organic coating on the surface of a metal crystal core (see Figure 12 (b)), which inhibits the growth of copper. Therefore, the growth of copper is relatively uniform, which can effectively reduce the particle size and improve the morphology to a certain extent. According to Table 4, the particle size of electrodeposited copper in different electrolytes can also prove the above conclusion. According to Table 4, the particle size of copper electrodeposition in this electrolyte is much smaller than the values reported by V.M. Maksimović [44]. This difference may be due to the use of ultrasonic dispersion in our experiments. There are literature reports [45] that ultrasonic dispersion can effectively reduce the agglomeration of copper powder.

Table 4 The particle size distribution of copper when the current density is 0.1 A/cm^2, T = 25 ℃, and pH = 2.1 for electrolytes with 0.1 g/L Tween 80, 0.1 g/L Tween 80 + 0.2 g/L SDS, and 0.1 g/L Tween 80 + 0.8 g/L SDS.

Solution	**0.1 g/L Tween 80**	**0.1 g/L Tween 80+0.2 g/L SDS**	**0.1 g/L Tween 80+0.8 g/L SDS**
Particle size(nm)	1000	2400	800

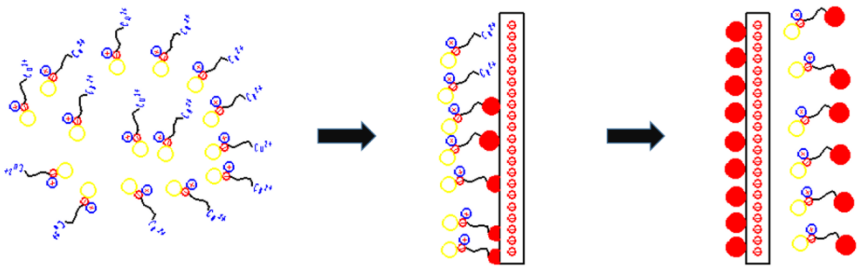

Figure 12. (**a**) Model of the copper powder formation mechanism at T=25℃ and pH=2.1 and with a 0.2 g/L SDS + 0.1 g/L Tween 80 mixed solution.

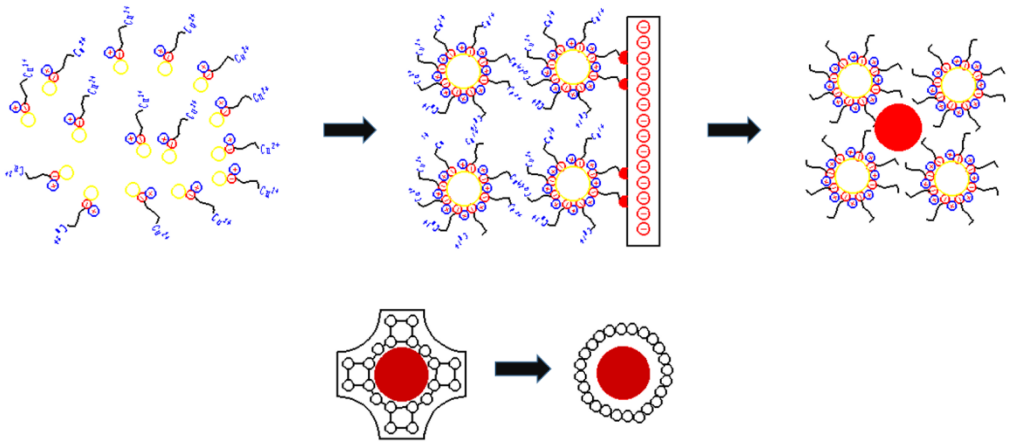

Figure 12. (b) Model of the copper powder formation mechanism at T=25℃ and pH=2.1 and with a 0.8 g/L SDS + 0.1 g/L Tween 80 mixed solution.

4. CONCLUSIONS

The effect of surfactants concentration (Tween 80, SDS) on copper electrode position was investigated in the sulfate electrolyte. According to the LSV curves, it can be found that the deposition potential decreases from -0.16 V to -0.18 V, which verifies that the long molecular chain surfactant can promote the cathodic polarization. Because the surfactant of the spherical micelles (0.1 g / L Tween 80 + 0.8 g / L SDS) can weaken the cathodic polarization, the deposition potential changes from -0.16 to -0.14 v. From the CA curves, it can be inferred that the surfactant with long molecular chain surfactants inhibits nucleation, while the surfactant of spherical micelle promotes nucleation. Meanwhile, the calculation of nuclear dynamics and EIS indicates that the surfactant with long molecular chain surfactant increases the resistance of the surfactant film on the electrode surface and inhibits the nucleation of copper, while the surfactant with spherical micelles can reduce the resistance of surfactant film on the electrode surface and promote the nucleation of copper. In addition, the surfactant can enhance the oxidation resistance of copper powders, and inhibit the growth of copper powders to improve the morphology.

AUTHOR CONTRIBUTIONS

H.J. and Y.W. conceived and designed the experiments; S.D., J.L. and X.L. performed the experiments; S.D. wrote the paper.

FUNDING

This work was supported by the Natural Science Fund of Liaoning Province (2020-BS-226, 2019-ZD-0278), the University of Science and Technology Liaoning Talent Project Grants (601011507-14), and the University of Science and Technology Liaoning Graduate Education Reform and Technology Innovation and Entrepreneurship Project (LKDYC201901).

ACKNOWLEDGEMENTS
This experimental material is supported by the University of Science and Technology Liaoning 2019 Graduate Science and Technology Innovation Project.

CONFLICTS OF INTEREST
The authors declare no conflicts of interest.

References

1. K. Zhuo, C.Y. An, P.K. Kannan, N. Seo, Y.S. Park and C.H. Chung, *Korean J. Chem. Eng.*, 34(2017)1483.
2. S.S. Wang, L. Liu, *J. Hazard. Mater*., 340(2017)445.
3. T.M.S. Rosbero, D.H. Camacho, *J. Environ. Chem. Eng*., 5(2017)3.
4. I. Hass, S. Shanmugam, A. Gedanken, *J. Phys. Chem*. B, 110(2006)16947.
5. W. J. Stepniowski, M. Moneta, K. Karczewski, M. Michalska-Domanskad, T. Czujko, J.M.C. Mol and J.G. Buijnsters, *J. Electroanal. Chem*., 809(2018)59.
6. A. Dianat, H. Yang, M. Bobeth, G. Cuniberti, *J. Appl. Electrochem*., 48(2018)211.
7. C. Ramirez, J.A. Calderón, *J. Electroanal. Chem*., 765(2015)132.
8. C. Reller, R. Krause, E. Volkova, B. Schmid, S. Neubauer, A. Rucki and M. Schuster, *Adv. Energy Mater.*, 7(2017)12.
9. Y.C. Tseng, H. Lee, Y.H. Nga, S.P. Feng and C.M. Chen, *J. Electron. Mater*., 47(2017)27.
10. S. Sengupta, A. Patra, S. Jena, K. Das and S. Das, *Metall. Mater. Trans*. A, 49(2018)920.
11. M.Y. Abyaneh, V. Saez, J. González-García, T.Z. Mason, *Electrochim. Acta*, 55(2010)3572.
12. D. Vasilakopoulos, M. Bouroushian, N. Spyrellis, *Electrochim. Acta*, 54(2009)2509.
13. J. Xue, Q. Wu, Z. Wang, S. Yi, *Hydrometallurgy*., 82(2006)154.
14. M.G. Kim, J.H. Paik, Y. Tak, *J. Nanosci. Nanotechnol*., 16(2016)10639.
15. S.W. Jiang, L. Yang, J.N. Pang, H. Lin and Z.Q. Wang, *Surf. Coat. Technol*., 286(2015)197.
16. Y. Liu, J. Gu, J. Zhang, F. Yu, J. Wang, N. Nie and W. Li, *RSC Adv*., 5(2015)9745.
17. W. Lou, W. Cai, P. Li, J Su and Y Zhang, *Powder Technol*., 326(2018)84.
18. R.K. Nekouie, F. Rashchi, N.N. Joda, *Powder Technol*., 237(2013)554.
19. J.W. Zheng, H.B. Chen, W. Cai, L. Qiao, Y. Ying, W. Li, J. Yu, L. Jiang and S. Chen, *Mater. Sci. Eng.*, B, 224(2017)18.
20. W. Jin, J.L. Su, *J. Electrochem. Soc*.,164(2017)723.
21. C.H. Huang, *Water Res*., 29(1995)1821.
22. N. Yoshii, K. Fujimoto, S. Okazaki, *J. Mol. Liq.*, 217(2015)99.
23. R. Chandran, R. Pandey, A. Mallik, *Mater. Lett*., 160(2015)275.
24. S.M.L. Baghal, A. Amadeh, M.H. Sohi, S.M.M. Hadavi, *Mater. Sci. Eng*., A, 559(2013)583.
25. Nekouie, F. Rashchi , N.N. Joda, *Powder Technol*., 237(2013)554.
26. M. Sima , I. Enculescu, M. Sima, E. Vasile and T. Visan, *Surf. Interface Anal*., 40(2008)561.
27. D. Myers, Surfactant Science and Technology, A, John Wiley & Sons, Canada 2006.
28. J.B. Raoof, S.R. Hosseini, S. Rezaee, *Electrochim. Acta*, 141(2014)340.
29. M. Eslami, H. Saghafian, F. Golestani-Fard, A. Robin, *Appl. Surf. Sci*., 300(2014)129.
30. B. Scharifker, G. Hills, *Electrochim. Acta*, 28(1983)879.
31. K. Raeissi, A. Saatchi, M.A. Golozar, *J. Appl. Electrochem*., 33(2003)635.
32. D. Grujicic, B. Pesic, *Electrochim. Acta*, 47(2002)2901.
33. R. Krumm, B. Guel, C. Schmitz, G. Staikov, *Electrochim. Acta*, 45(2000)3255.
34. A. Radisic, J.G. Long, P.M. Hoffmann, P.C. Searson, *J. Electrochem. Soc*. 148 (1) (2001) C41.
35. M. Palomar-Pardavé, B.R. Scharifker, E.M. Arce, M. Romero-Romoa, *Electrochim. Acta*, 50(2005)4736.

36. S. Popescu, C. Ungureanu, A.M. Albu, C. Pirvu, *Prog. Org. Coat*., 77(2014)1890.
37. T.J. Licona-Sánchez, G.A. Alvarez-Romero, L.H. Mendoza-Huizar, C.A. Galán-Vidal, M.Palomar-Pardavé, M. Romero-Romo, H. Herrera-Hernández, J. Uruchurtu and J.M. Juárez-García, *J. Phys. Chem. B*, 114(2010)9737.
38. J. Ross Macdonald, Donald R. Franceschetti. *J. Electroanal. Chem*., 99(1979)283.
39. F. Hu, K.C. Chan, *Mater. Chem. Phys*., 99(2006)424.
40. H. Xu, J. Wu, C. Li, J. Zhang and J. Liu, *Electrochim. Acta*, 165(2015)14.
41. H. Ashassi-Sorkhabi, B. Rezaei-Moghadam, *J. Environ. Chem. Eng*., 5(2017)3.
42. A.S. Kamble, V.L. Patil, B.B. Sinha, S.A. Vanalakar, S.L. Dhere, S.S. Kale, P.S. Patil and J.H. Kim, *J. Solid State Electrochem*., 21(2017)2649.
43. W.Y. Ko, W.H. Chen, C.Y. Cheng, K.J. Lin, *Nanoscale Res. Lett*., 4(2009)1481.
44. V.M. Maksimović, L.J. Pavlović, M.G. Pavlović and M.V. Tomić,*J. Appl. Electrochem*., 2009, 39(2009)2545.
45. L. Fathyunes, J. Khalil-Allafi. *Ceram. Int*., 43(2017)16.